MEASUREMENT TECHNIQUES FOR FLOW DIAGNOSTIC IN ITAM IMPULSE WIND TUNNELS

Prof. A.M. Kharitonov, Chief Scientist,
Khristianovich Institute of Theoretical and Applied Mechanics SB RAS, Russia

Introduction

Like blowdown wind tunnels, impulse facilities are used to measure the angles of attack, roll, and yaw, coefficients of the drag and lift forces, and aerodynamic moments acting on the wings and fins of the flying vehicle.

Strength, vibration, and strain calculations of flying vehicles require measurements of distributed aerodynamic forces over the surface under different conditions of motion. This complicated and labor-consuming problem is very important in studying the structure and conditions of formation of the resultant forces and moments.

Hypersonic flight is characterized by extremely high stagnation temperatures. Under these conditions, the surface of the flying vehicle is subjected to significant aerodynamic heating owing to compression and friction in the ambient medium. Therefore, measurements of temperature and heat-flux distributions on the model surface are necessary for calculating the strength and strains of the flying vehicle and its cooling systems.

Requirements to sensors and equipment in impulse wind tunnels, as well as in long-duration wind tunnels, are determined by the nature of the phenomenon under study. For instance, measurements of turbulent velocity oscillations require fast-response equipment and sensors with a resolution of $10^{-4} \div 10^{-5}$ s.

Aerodynamic forces and moments, pressures, and heat fluxes are measured by fast-response strain-gauge transducers and calorimetric sensors possessing high accuracy and sensitivity, and also fast-response equipment.

Studies of the flow structure involving measurements of parameter fields and panoramic patterns stimulate extensive applications of optical methods for both qualitative and quantitative measurements. In these situations, almost instantaneous flow patterns have to be measured, which is extremely important for studying the fine structure of the flow.

Experimental aeromechanics, like other fields of science and engineering, makes use of the latest advantages in electronics, optics, and informatics. Novel optical methods, such as laser techniques, holography, tomography, etc., have gained particular popularity in test facilities.

1. Methods of measurement of aerodynamic characteristics

It is well known [1–3] that the basic measurement device for wind tunnels, which allows determining the components of the total aerodynamic forces and moments, is the aerodynamic balance on which the models are mounted. Tests in impulse facilities are mainly performed with the use of low-inertia strain-gauge aerodynamic balances. As the angle of attack of the model in a strain-gauge balance is changed by turning the model together with the sting, the components of the total aerodynamic force and moment are measured in a model-fitted coordinate system. By connecting the strain-gauge sensors mounted at different points into measurement bridges, one can make the output signal of each bridge depend mainly on one

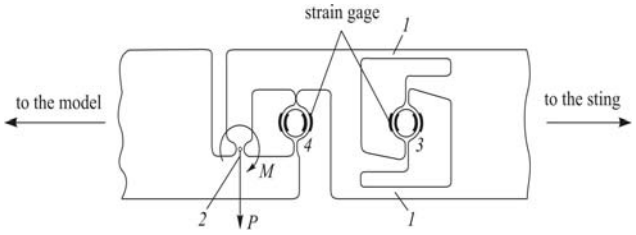

Fig. 1 Cantilever strain-gauge system

component of the aerodynamic load acting on the model. An example of force and moment measurements with the use of a cantilever bar is shown in Fig. 1.

The elastic element consists of two parallel plates 1 connected by rigid elements (elastic parallelogram) and serves for kinematic insulation of the force *P*. An elastic hinge 2 serves to "insulate" the moment *M*; elastic measuring elements 3 and 4 are used to measure *P* and *M,* respectively.

Thus, by choosing an appropriate geometric shape of the elastic element, one can reach a situation where the strain induced by the measured component is significantly greater than the strains caused by other components. The residual mutual effects can be reduced or completely eliminated by compensation circuits based on analytical properties of the measurement bridges including strain-gauge sensors.

To improve the measurement accuracy, the strain gauges can be placed in a larger number of sections. In this case, the number of equations exceeds the number of unknowns, and the normal force *Y* and pitching moment M_Z are found by the least squares technique as

$$Y = k\frac{n\sum x_i\Delta U_i - \sum x_i \sum \Delta U_i}{n\sum x_i^2 - \left(\sum x_i\right)^2}, \qquad M_Z = k\frac{n\sum x_i\Delta U_i - \sum x_i \sum x_i\Delta U_i}{n\sum x_i^2 - \left(\sum x_i\right)^2},$$

where n is the number of cross sections where the strain gauges are glued, x_i are the coordinates of these cross sections, and ΔU_i are the output signals of the measurement bridges.

In ITAM impulse facilities usually we use different type of strain-gage balances. It dependence from task to be solved. To measure the force and moment independently one can use the measurement bridge as a simple calculation device. To determine the force or moment from the measured signal of the strain-gauge bridge, one has to know conversion factors found by balance calibrations on special calibration rigs where the balance is mounted.

In hypersonic tunnels with heating, under conditions of variable temperatures, it is also necessary to perform thermal calibrations in the range of 10 to 100ºC to determine fluctuations around the zero value.

In short-duration wind tunnels, in addition, dynamic calibrations are necessary. Determining the forces and moments acting on the model tested in impulse facilities by the strain-gauge balance requires the dynamic character of the recorded signal to be taken into account. Various methods of data processing are used for this purpose: 1) averaging technique; 2) analytical method; 3) statistical method; 4) and simplified statistical method [4]. The averaging technique requires a sufficiently long time of wind-tunnel operation, so that oscillations caused by initial shock loads could decay and a comparatively long time period with constant flow parameters. Even if these conditions are satisfied, however, there remains an uncontrollable systematic error. Three other methods require measurements of accelerations at certain points with the use of accelerometers. The analytical method faces difficulties in determining the mass, the center of mass, and the moments of inertia of the part of the system that participates in motion. Statistical methods require the periods of system oscillations to be correlated with the test time (time window of a steady flow), which may impose additional restrictions on the model mass.

At conducting the dynamic calibrations of strain-gage balances we usually make an assumption that the response of the strain-gage balance registered in time is described by ordinary differential equations with constant coefficients with an assumption that the stress/strain relationship is described by the Hooke's law.

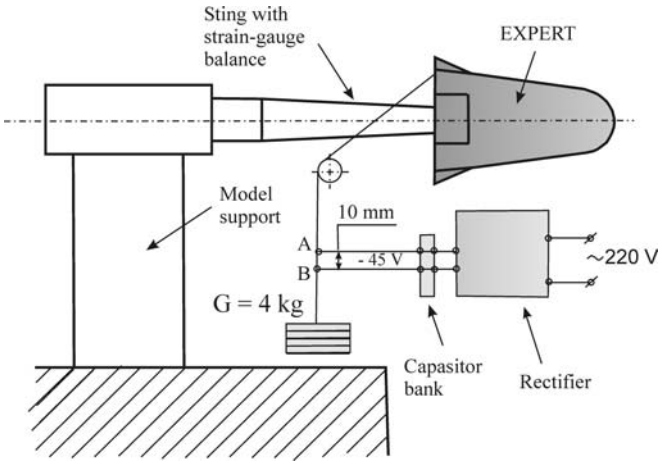

Fig. 2

In this case, obtaining experimentally the response of the system «model +sting+ strain-gage balances» to unit loads, we can define a system of integral equations for reconstructing the acting loads as a function of time on the basis of the measured response.

Therefore, a new method was proposed [5], which is devoid of most of these drawbacks and takes into account the dynamics of model motion. In this case, the strain-gauge balance together with the model should be dynamically calibrated, i.e., the response of the system consisting of the model plus the sting plus the strain-gauge balance should be measured. Based on the responses of the strain-gauge balance in time a system of integral equations for retrieving the loads is derived. All methods imply static calibrations. As an example, dynamic calibration of the strain-gauge balance together with the EXPERT model is described below.

To conduct dynamic calibrations, the model with the sting and strain-gauge balance is mounted on a support attached to a massive foundation. A sketch of the test bench for dynamic calibrations is shown in Fig. 2

The model with the sting and strain-gauge balance is mounted on the test bench. A 4-kg load was suspended on the model on a nichrome wire 0.3 mm in diameter. The wire was fixed on the model at different points of the base section, and necessary loads of different magnitudes and sign for all components of the balance were generated by changing the wire direction.

The voltage oscillogram consists of sinusoidal arcs with a frequency of 100 Hz without smoothing, i. e. the voltage passes through zero points. After system start-up, current is supplied to the segment AB of the wire enclosed into a ceramic tube by switching on the rectifier. This segment of the wire burns, like a fuse link, and the load is instantaneously released from the balance. At least six tests with different combinations of loads were performed.

Such a method of reconstructing the time-dependent forces acting on the model does not impose any restrictions on the model mass.

To verify the assumption on possible electromagnetic noise induced on the strain-gauge balance by a powerful current pulse, a special experiment was performed, where the load was attached close to the model rather than suspended on the model. After wire burning, the oscillogram displayed no effect on the Y component of the strain-gauge balance. Hence, no electromagnetic noise was induced. As an example, Fig. 3 shows the signals of the tangential and normal components of forces for one variant of loading. The section with a constant level of the signal at $t < 730$ ms corresponds to the loaded state, then there follows unloading (burning of the wire) and decay of oscillations of the model-sting system. To take into account the dynamic error of the strain-gauge balance, a special technique and software for

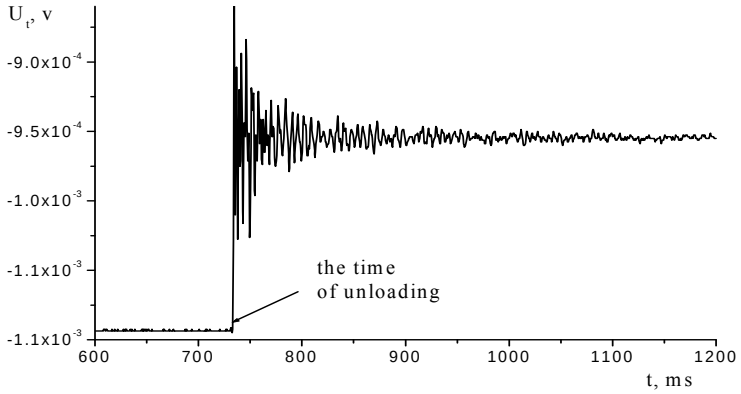

Fig. 3

determining the forces and moments in the class of piecewise-constant functions were developed [5]. The computed and measured responses of the strain-gauge balance of the aerodynamic coefficients for the reference model HB-2 for the test conditions: flow Mach number $M_\infty \approx 9{,}5$ and angle of attack $\alpha = 6^\circ$ are in good agreement.

2. Pressure-measurement techniques

The pressure distributions on the models reveal the physical pattern of the flow and give better understanding of formation the lifting properties of the vehicle. Like in blowdown wind tunnels, one of the basic and most widely spread methods of aerodynamic experiment in impulse facilities is the measurement of pressure on the surfaces of flying vehicle models and in their vicinity. Such measurements are extremely complicated and labor-consuming, because they have to be made in a large number of points. In impulse facilities, it is also necessary to take into account the dynamic character of the recorded signals, whereas it is impossible to use inertial pneumatic tubes, which require additional time for pressure equalization. Therefore, pressure measurements on models in impulse facilities necessitate to use of miniature electrical probes with a fairly wide range of frequencies, which are flush-mounted on the surface or built into the model body. In this case, reaching required high accuracy of static pressure measurement is a difficult task, because the errors of static pressure measurement are determined not only by the accuracy of the measurement instruments used but also by the errors of manufacturing of the models, nonuniformity of the velocity field in the test section, and instability of flow parameters in time.

Various methods and instruments for static and total pressure measurements have been extensively considered in the literature, for instance, in [2, 3, 6÷9]. Therefore, we give only a brief description of some probes and devices used in ITAM impulse facilities.

Electrical pressure transducers are devices used to convert the strain of the elastic sensor perceiving the measured pressure into the electric signal. The electrical pressure transducers are sufficiently small, provide high measurement accuracy, and are the only means for registering unsteady pressures in unsteady or slowly changing flows. Such probes are indispensable for research in hypersonic short-duration wind tunnels, where the measurements by other devices are impossible because of a large time lag. It is extremely important that the natural frequency of the elastic element in such a probe is several times higher than the frequency of the measured pressure.

Almost all pressure transducers used in aerodynamic experiments can be classified into three groups: strain-gauge, inductive and piezoelectric pressure probes.

A strain-gauge pressure probe is an elastic element (membrane) in a sealed casing, which perceives the measured pressure or the pressure difference. Wire, foil, or semiconductor strain gauges are glued or sprayed onto this elastic element. The change in pressure in the probe casing induces deformation of the elastic element and, as a consequence, a change in electrical resistance recorded by special devices. A sketch of such a probe is shown in Fig. 4. Pressure probes of this type have a small size (diameter of 1.5 ÷ 8 mm) and can be flush-mounted on the model surface. Strain-gauge probes with a known resistance are included into the arms of the measurement half-bridge whose disbalance, depending on the membrane bending, corresponds to the measured pressure. The error of such probes stays within 0.2 ÷ 0.3%.

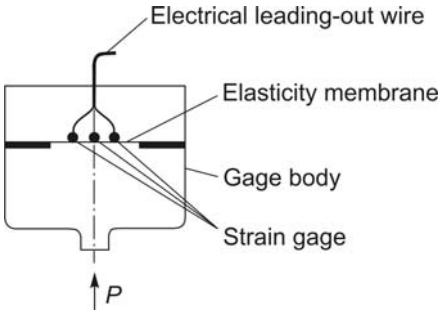

Fig. 4 Sketch of strain-gauge pressure probes

Inductive pressure probes are based on the property of coils to change their inductance as a metallic rod moves inside the coils. The operation principle of the differential inductive probe implies that the motion of the membrane under the action of the measured pressure alters the air gaps between the membrane and the magnet core of the coils (one gap increases and the other gap decreases). This involves the corresponding changes in magnetic resistances to the flow generated by these coils. The reactive resistance of the coil depends on the magnitude of the gap induced by the change in pressure acting on the membrane. Including the coil into the bridge measurement circuit induces an electromotive force of bridge disbalance, proportional to the pressure difference on the membrane, and corresponding current at the system output $\pm\Delta P = f(\Delta Z)$. Here Z is the total electric resistance determined as $Z = R + j\omega L$, where R is the resistance of the coils, $j\omega L$ is the reactive component of magnetic resistance, ω is the angular frequency of flow variation, equal to the frequency of the current feeding the probe, and L is the inductance of half of the probe. A sketch of the pressure probe operating on this principle is shown in Fig. 5. The required sensitivity (ratio between the increment of inductance to the change in the measured pressure) is reached by choosing an appropriate membrane thickness.

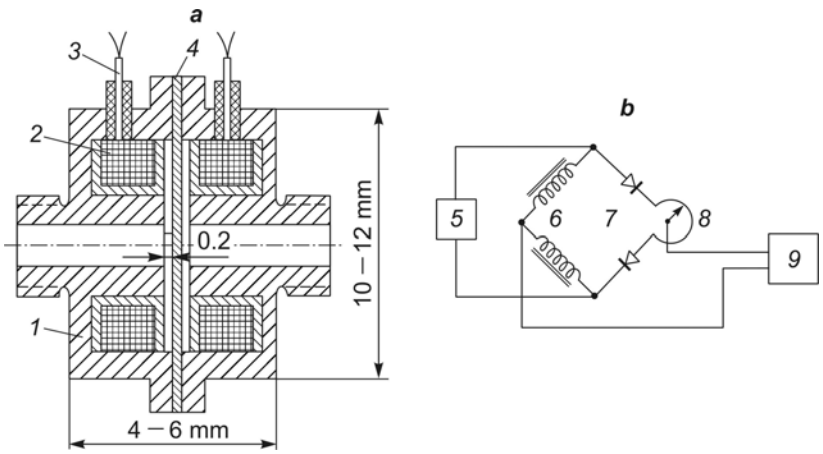

Fig. 5 Structure (*a*) and bridge circuit (*b*) of the inductive pressure probe: *1* – casing; 2 – coil; *3* – outputs of the electric signal of the coil; *4* – membrane soldered to the casing; 5 – source voltage; *6* – differential inductive probe; *7* – rectifiers; *8* – adjustment of the zero point; 9 – oscillograph.

Commercial inductive probes for measuring the absolute and differential pressures in the range from 0.01 to 0.6 MPa and from 0.14 to 1 MPa are available. A substantial advantage of these probes is their small size; hence, they can be used to measure unsteady pressures in the range of frequencies up to 5 kHz. Depending on the measurement system, the accuracy can reach 0.5% of the measured quantity if the

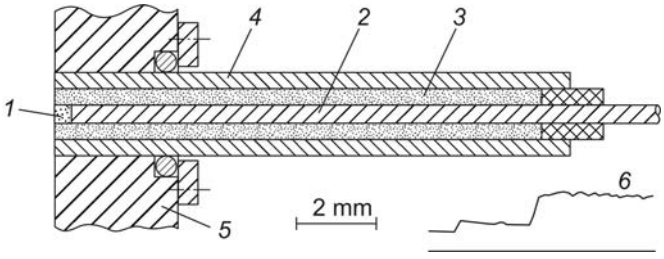

Fig. 6. Sketch of the piezoelectric pressure probe: *1* – piezoelement; *2* – rod; *3* – vibration-insulating material (wax); *4* – casing; *5* – model wall; *6* – typical pressure oscillogram

probes are individually calibrated.

Piezoelectric pressure gauges are based on the effect discovered by the Curie brothers back in 1880. This effect implies that an electric charge appears on the piezocrystal faces if the piezocrystal is subjected to forcing whose direction coincides with the crystallographic axis. Thus, applying pressure to the piezocrystal leads to formation of an elastic wave propagating in the crystal with a velocity of sound. The electric discharge on the piezoelement liner is proportional to the strain determined by the measured pressure. The resolution of the pressure probe primarily depends on the time needed for the elastic wave to cover the piezoelement thickness, which can reach ~10^{-7} s for a thickness of ~ 1 mm. Vibration insulation of the probe casing plays an important role.

An example of the piezoelectric probe made of ceramic piezomaterials [10] is shown in Fig. 6. The operation principle of such a probe is based on "deflection" of the elastic wave arising in a cylindrical piezoelement 1 into a long rod 2 made of a material whose acoustic resistance is identical to that of the piezoelement material. To attenuate the effect of vibrations of the casing 4 and model walls 5, the probe is filled by bee-wax 3.

The rod serves as one of the electrodes in the system. The other electrode in the form of a thin wire is soldered to the silver-plated outside end face of the piezoelement by Wood's alloy. The voltage is measured by an electronic amplifier connected to the output of the probe electrode.

Piezoelectric probes allow measuring unsteady pressures in flows with frequencies up to 100 kHz and higher. They possess high mechanical strength and ensure reliable operation in the ranges of pressures from 1mbar to 10 kbar and temperatures from –240 to +260°C. transducer. Piezoelements are usually quartz crystals. The error of shock-wave calibration of such probes is usually within 3% of the measured value.

One of the options of the piezoelectric pressure probes is a piezooptical pressure [11]. The operation principle of such probes is based on the use of the piezooptical effect: changes in optical properties of a transparent material under mechanical loading. Such piezooptical pressure transducers are highly sensitive. If the elastic element is made of molten quartz, the sensitivity of such a probe is several orders higher than the sensitivity of the strain-gauge probes. The structure of pressure probes operating on this principle is shown in Fig. 7.

It consists of a casing *1*, where a sleeve *3* is fixed by a coupling nut. A bellow valve *4* is soldered to the sleeve. An elastic element 6 in the form of a glass bar with a square cross section is attached to the bottom *5*. A cylinder *7* fixed by a screw *8* is glued to the other end of the elastic element. On one side of the elastic element, there is a sleeve *9* with a light-emitting diode (LED) *10*, a Polaroid polarizer *11* and a phase plate *12* being glued to the inner

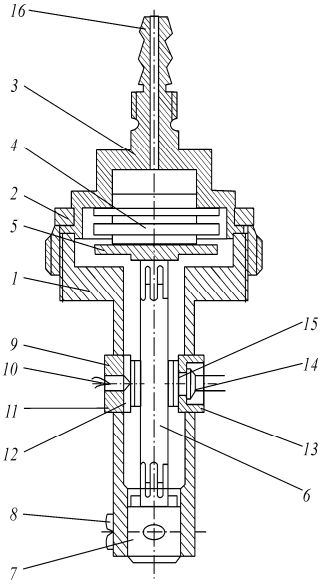

Fig. 7. Sketch of the piezooptical pressure transducer

side of the sleeve. On the other side, of the elastic element, a sleeve *13* with a differential photodetector *15* is inserted into the casing. Two Polaroid analyzers *14* with mutually perpendicular polarization planes are glued onto the inner end face of the sleeve *13*. The light emitted by the LED passes through the polarizer, phase plate, elastic element, and analyzers, and reaches the differential photodetector *15*. The bellow-valve volume communicates with a pressure hole on the model through a fitting *16*. The measured pressure generates a compressive stress in the elastic element (excess pressure) or a tensile stress (if the pressure is below the atmospheric value). The output voltage of the bridge with a differential photodiode is changed in proportion to the difference between the measured and reference pressures.

Such piezooptical pressure probes are designed for a range of pressures $+10^5 \div -0.9\times10^5$ Pa. The influence of temperature on metrological characteristics of the probe is reduced by using temperature-compensation schemes, which ensure oscillation of the temperature dependence of sensitivity coefficients of the probes from 0.09 to 0.24% per degree. The drift of the zero point due to instability of temperature characteristics of film Polaroid polarizer and photo detectors can also be reduced by using compensation schemes to 0.05% per degree.

Method of surface pressure measurement by pressure-sensitive coatings. To retrieve the local pressure, one has to perform calibrations, e.g., by registering the data of static pressure sensors located on the surface. The ratio between the luminescence I and the local pressure can be presented as [9], where the subscript 0 refers to known conditions, and the coefficients A and B depend on local temperature $\frac{I_0}{I} = A(T) + B(T)\frac{p}{p_0}$.

Hence, to use this method for surface pressure measurements, one has to know local temperature, while variations of the latter lead to uncertainties in the measured pressure. Therefore, the method of pressure-sensitive coatings requires careful calibrations of the models in special chambers with controlled temperature and pressure. These calibrations with different pressures yield the dependences A(T) and B(T). The error of measurements by this method also depends on the accurate knowledge of intensity I_0. In addition to difficulties in providing uniform illumination of the entire surface, this intensity depends on fluctuations of power of the light source and deformation of model elements, which alters the flow velocity. Some of these effects can be taken into account by introducing appropriate corrections. The method of illumination duration is sometimes used. The intensity of fluorescent light emitted by the surface changes in time as $I = I_{in}e^{-kt}$, where I_{in} is the initial intensity and $k = k_{rad} + k_{exch} + k_{quench}$ (the coefficients k_{rad}, k_{exch}, and k_{quench} characterize the changes due to radiation, other exchange processes, and oxygen quenching, respectively). The intensity of fluorescent light is usually estimated on the basis of integral values measured in two time intervals and then is calculated by the formula $\int_T^{2T} Idt \Big/ \int_0^T Idt = e^{-kT}$, which is sensitive to pressure and temperature but insensitive to illumination intensity. The coefficient k_{rad} is almost insensitive to temperature, whereas the coefficient k_{exch} depends on the absolute temperature as $k_{exch} \sim e^{-\Delta E/RT}$, where ΔE is the activation energy of the process and R is the universal gas constant. Hence, it seems preferable to use materials with comparatively high values of ΔE as pressure-sensitive coatings, because they are less temperature-dependent.

Thus, pressure-sensitive coatings (luminophores) are successfully used to visualize the distributions of surface pressures, separation regions, and positions of shock waves on various surfaces.

3. Methods of temperature measurements

The temperature is measured by various devices with different configurations, whose operation is based on different physical effects. Gas thermometers, mercury thermometers, resistance thermometers, thermocouples, optical pyrometers, and a number of spectroscopic methods have gained widespread applications for accurate measurements of temperature in a wide range. These devices and optical instruments have to be carefully calibrated, based on a single standard temperature scale.

The most general approach to estimating the interaction between the temperature gauge and the subject of research divides all measurement methods into two groups: contact and contact less methods. A detailed description of various measurement methods and instruments can be found in [1–3, and 9].

Contact methods of temperature measurement. The following types of temperature gauges are most widely used: resistance thermometers and thermocouple. An important advantage of the thermocouples considered is the possibility of temperature measurements within wide ranges. For high temperatures above 1000°C platinum-rhodium wires ~0.1 mm in diameter are used. As the specific heat of the junctions is low, the thermal inertia is also low, and it is possible to measure rapidly changing temperatures. The small size of the junction makes it possible to perform temperature measurements practically at a point.

Contactless methods of temperature measurement. If it is necessary to achieve a fast response and better measurement accuracy or to measure temperatures above 1500 K, contact less optical methods are used. The use of small-size thermocouples or resistance thermometers for these purposes is restricted by the time needed to heat the sensor ($10^{-3}\div10^{-4}$) s and by possible influence of various processes at the gas-solid interface.

Therefore, spectroscopic methods are used, which ensure measurements of gas temperatures above 1500 K within 1% with a time resolution of $10^{-6}\div10^{-7}$ s. These methods are based on the laws of equilibrium radiation [10] applied in a number of spectroscopic methods of measuring flame temperatures and similar objects of continuous media.

Contact less methods of temperature measurement include also the known method of optical pyrometers, which allows temperature measurements above 1600°C. As it is well known this method is based on using the laws of thermal emission of a blackbody [15].

In practice of aerophysical experiments, it is often necessary to determine the temperature fields, i.e., panoramic image of isotherms. Such information can be obtained by means of using panoramic methods of temperature measurement i.e., the use of various thermal indicators for example liquid crystals or infrared imaging. Liquid crystals (LC) are widely used for visualizing temperature fields in the range from –10 to +200 °C. The color of the LC film applied onto the model surface changes in the visible range from red to violet as the temperature changes from fractions of a degree to 50°C. These properties of liquid crystals allows visualization of the transition from a laminar to a turbulent flow, changes in temperature caused by shock-wave interaction on model surfaces, and other phenomena. Based on the change in color, the temperature distribution on the surface can be visualized with a high resolution (~0.025 °C). With allowance for LC reversibility, fast operation, and ability to work at room temperature, they seems to be extremely promising tools for aerophysical experiments.

Prof. Zharkova [16, 17] developed a thermal indicator material based on liquid crystals encapsulated into a hydrophobic polymer. An undoubted advantage of this material is reversibility of its color-temperature characteristics. In practice, this means that such thermal indicators can be used many times without repainting the model. This is evidenced by

reflection spectra obtained after five heating-cooling cycles, which are practically identical. The dynamic error of thermal indicators encapsulated into a polymer is ~50 ms.

Usually we used a unique and comparatively simple method allows quantifying the temperature fields with the use of LC coatings of the flow [18]. The examined surface *1* with the LC coating (Fig. 8) is illuminated by a projector *2* through a transparent *3*, which is a set of straight-line regular black and white bands. The image of these bands is focused onto the object surface, and the projector lens and examined surface are separated by an optical prism *4*, which performs spectral decomposition of the band with respect to the coordinate orthogonal to their direction. Then the position of the bands is different for different wavelengths. The image of the examined surface in reflected light is recorded by a TV camera *5* and is fed to a computer.

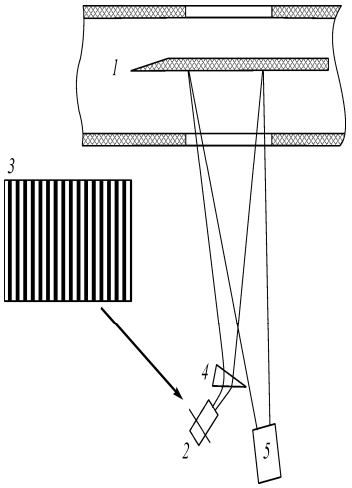

Fig. 8 Registration of temperature fields by LC coatings: *1* – examined surface; *2* – projector; 3 – transparent; *4* – optical prism; *5* – TV camera.

The resultant image resembles an interferograms in finite fringes and the shift of the bands is clearly registered even if a black-and-white camera is used.

Relations derived in [18] definitely demonstrate that the bands for regions with temperatures corresponding to a certain maximum frequency of selective reflection have the maximums of intensity in the center of light (for this frequency) regions of the modulating bands. To increase the accuracy of the dynamic range and the contrast of the images obtained, one can use special calibration images (several images being registered at different temperatures). This allows determining the positions of the maximum of the bands and, hence, the dependence of the band shifts on temperature.

Thus, the use of calibration images before or after the basic experiment makes it possible to allow for effects related to properties of the LC coating, specific features of illumination, and the optical scheme used.

4. Methods of heat-flux measurement

As it follows from the Fourier law, the heat flux is a derivative of the amount of heat with respect to time $q = \frac{dQ}{dt}$. This is a vector characterized by a direction, in addition to the absolute value. Aerophisical experiments often involve both discrete heat-flux probes and methods $q(x, y, z, t)$, which allow determining both the mean and local instantaneous values.

Calorimetric method of heat-flux measurement implies the use of a probe of the type of an auxiliary wall. The essence of the method is based on placing a wall (calorimeter) with a known thermal conductivity on the path of the heat flux to be measured. Such a heat-flux probe based on the longitudinal Seebeck effect is a flat, cylindrical, or spherical element (calorimeter) aligned normal to an isothermal surface so that the heat-flux density is constant within the area occupied by the sensor. As an example, Fig. 9 shows a sketch of a thermocouple-type calorimetric heat-flux probe developed at ITAM [3]. The basic element of the probe is a calorimeter *1* made in the form of a copper disk 2.5 mm in diameter and 0.2 mm thick, which is fixed in a thermal insulator *2* near the stagnation point of the hemisphere of the

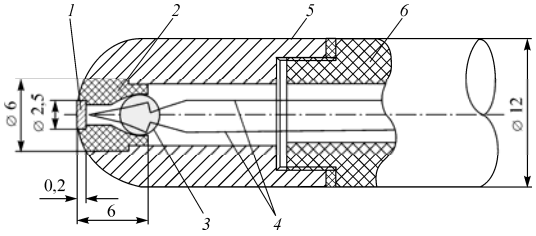

Fig. 9 Heat-flux probe: *1* – calorimeter, *2* – thermal insulator, *3* – glue, *4* – thermocouple wires, *5* – probe casing, *6* – insulating insert

probe casing *5*. The calorimeter *1* is glued to the thermal insulator *2* made of a low-heat-conducting material by a high-temperature adhesive.

With the use of a special technology, the junction of a copper-Constantan thermocouple is welded to the inner surface of the calorimeter; the thickness of the thermocouple wires is 50 μm. by means of electric-discharge welding, these wires are connected to appropriate thermocouple wires 200 μm in diameter. The thermocouple junction *3* is attached to the inner side of the disk. It generates a thermal emf proportional to the temperature difference in the direction of the heat-flux vector. The thermocouple outputs 4 are connected to a device that registers the emf induced by heating of the thermocouple junction. Based on the shape of the curve $U = f(t)$ in the oscillogram, one can determine the steepness of the curve characterizing the growth rate of the signal: the ratio of the quantity characterizing the increase in the output voltage U to the corresponding time interval based on the prior calibrations one can find the heat flux from the gas to the calorimeter. The elementary theory of such a probe is based on the steady-state solution of a boundary-value heat-conduction problem for an infinite plate. According to this solution, the heat flux in an arbitrary cross section of this plate is constant and equal to $q = \lambda \dfrac{\Delta T}{\delta}$ where $\lambda, \delta, \Delta T$ are the thermal conductivity, thickness of the calorimeter, and difference in temperature on the opposite ends of the calorimeter.

The use of such probes in impulse facilities requires additional dynamic calibrations. The available experience shows that dynamic calibrations of the probes allow significant reduction of the measurement error. Hence, the conversion factors of heat-flux probes, which establish the relation between the heat-flux level and the temperature gradient in time, should be determined from the results of individual dynamic calibrations on special facilities.

Thus, the heat-flux value is determined by multiplying the derivative of voltage with respect to time by the conversion factor of the corresponding probe $q = \dfrac{dU}{dt} K \left[\dfrac{\text{mW}_\text{T}}{m^2} \right]$.

The root-mean-square deviations of the heat-flux levels in multiple measurements are 2–3 %. Then the total error including random and systematic errors reaches ~15 %.

The total error is caused by deviation of the geometric size from the nominal value, heat transfer to thermocouple wires, averaging of the temperature of the calorimeter surface, heating of the cold junctions of the thermocouples

As a whole, it should be always borne in mind that the error of heat-flux measurements by contact probes is caused by the difference in temperature between the probe surface and the ambient surface. Therefore, the heat flux onto the probe is not identical to the heat flux onto the surface in the absence of the probe. Strictly speaking, the probe signal is a characteristic of the heat flux onto the probe rather than onto the undisturbed surface. This error depends on the properties of a particular probe, which are determined by two characteristics: (1) ratio of the heat flux obtained in probe calibrations to the undisturbed heat flux and (2) probe signal (deviation of temperature) divided by the total difference in temperature between the undisturbed flow and the wall $\Delta T/\Delta T_\infty$.

Based on two-dimensional Navier – Stokes calculations of temperature fields in the vicinity of points with temperature discontinuity on the wall, it was found [19] that the error is determined by both the probe size and the temperature difference ΔT. The smaller the probe size, the smaller the error, but also the smaller the probe signal ΔT. Therefore, the choice of the probe to be used and its characteristics is a reasonable compromise between heat-flux distortions and errors in signal registration.

Gradient-type heat-flux probes. The operation principle of gradient-type heat-flux probes is based on the transverse Seebeck effect, namely, on the emergence of the transverse component of the electric field in a crystal with anisotropic thermal conductivity and thermal coefficient owing to heat-flux passing in a direction other than the directions of the principal axes of the crystal [20]. Under the action of an external heat flux, there arises an electric field in the anisotropic thermal element; the direction of the strength vector of this field (owing to anisotropy of the thermal conductivity and thermal emf coefficients) coincides with neither the vector of the external heat flux nor with the vector of the heat flux inside the anisotropic thermal element.

Thus, the transverse Seebeck effect acts in the x direction on the basis of the Fourier law. Therefore, there arises a thermal emf, which is linearly related to the heat-flux density and area of the anisotropic thermal element. The value of the thermal emf is determined by the choice of the angle, which is characterized by the degree of anisotropy of the chosen material. For bismuth, for instance, the optimal angle is $53^{\circ}24'$.

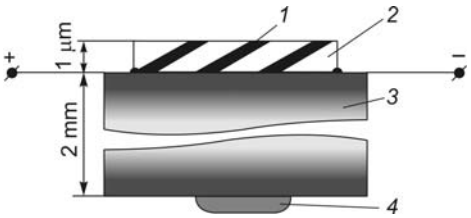

Fig. 10 ALTP sensor of the FORTECH HTS company: *1* – CuO_2, *2* – $YBa_2Cu_3O_7$-d, *3* – $SrTiO_3$ substrate, *4* – thermocouple.

Figure 10 shows a sketch of a heat-flux sensor based on an artificially anisotropic thermal element [20] which was developed and advertises an ALTP (atomic layer thermo pile) by FORTECH HTS Company. A film 1 μm thick with oblique layers is made of alternating superconducting layers of yttrium ceramics $YBa_2Cu_3O_7$-d *2* and semiconductor CuO_2 1. The film is applied onto a substrate 3 made of $SrTiO_3$ (strontium, titanium) 2 mm thick. The entire sensor has the form of a cylinder 6 mm in diameter. The volt-watt sensitivity of the ALTP sensors is 18.6÷26.6 mV/W, and the time constant is characterized by the Company as $\tau_{\min} = 10^{-6}$ s, which corresponds to the frequency of heat-flux variation equal to 300 kHz. These sensors are used to study hypersonic flows in impulse facilities [21]. The sensitivity of sensors made of bismuth is 5÷30 mV/W, and their time constant is $\tau_{\min} = 10^{-5}$ s. Calibration of such sensors up to the melting point of bismuth is performed by the absolute method, based on the Joule-Lenz heat flux. The calibrate curve of the gradient-type heat-flux sensor evidences that the characteristic of this sensor is linear for external pressures up to 30 MPa.

Method of determining heat fluxes with the use of thermal indicator coatings attracts the attention of researchers by the possibility of panoramic visualization of the heat-flux distribution on the model surface [22]. This method has a number of important advantages over methods with discrete probes: it allows one to measure the distribution of the local heat fluxes over the entire area observed and provides a large amount of information in each test. Test results are obtained in an illustrative and clearly readable form including in experiments the process filming; method allows identification of zones of strong and weak heat transfer.

For this method to be used, the model of an arbitrary configuration is made of a low-heat-conducting material. A thin layer of the temperature-sensitive coating (within 100 μm) is

applied onto the model to be tested, and the model is rapidly inserted into the flow. If the initial temperature of the model is lower that the temperature of the incoming flow, unsteady heating of the model surface occurs. The rate of model heating is determined by filming the color transition. The color is first changed in zones of high heat fluxes, which yields a visual pattern of surface heating. Based on the filming results (motion of the transition isotherm on the surface), one can calculate the heat-transfer coefficient. For this purpose, the thermal indicators should possess high-contrast changes in color, properties that allow their application as a thin layer onto the surface, and good adhesion to the surface. In addition, the material of the thermal indicator should have low thermal diffusivity to reduce heat migration and to ensure the local character of measurements. It should also be homogeneous, and its thermophysical properties should be stable. The effect of external factors other than temperature (heating rate, pressure, etc.) on the color transition should be negligible. All these requirements are satisfied by substances that change the optical properties of the surface (color, reflectivity, etc.) at a certain temperature. The primary candidates are liquid crystals and melting thermal indicators.

The specific heat flux to the model is usually found by solving of the generally accepted heat-conduction equation for a semi-infinite body. Thus, the data measured during the experiment are T, T_{in}, and $T_e = T_0$. At the time $t = 0$, the model is rapidly inserted into the flow, and filming is used to record consecutive positions of the isocaloric line on the model surface and the time t. The isocaloric line is simultaneously an isotherm displayed by the thermal indicator applied onto the model surface.

Knowing the distributions of the heat-transfer coefficient, one can determine the dimensionless Stanton or Nusselt numbers: $\mathrm{St} = \dfrac{\alpha}{\rho_\infty u_\infty c_p}$; $\mathrm{Nu} = \dfrac{\alpha d}{\lambda} = \dfrac{\beta d}{\sqrt{a\left(t - t_0\right)}}$.

For determining the Stanton numbers, one has prior to find the parameters P_∞ and T_∞ by using the gas-dynamic functions: $P_\infty = P_0 \pi\left(M_\infty\right)$ and $T_\infty = T_0 \tau\left(M_\infty\right)$. Thereby, $u_\infty = M_\infty a = M_\infty \sqrt{\kappa g R T_\infty}$ and $\rho_\infty = \dfrac{p_\infty}{R T_\infty}$.

A specific feature of thermal indicators is their melting under the action of the total applied heat flux beginning from the moment of model insertion into the flow, which is particularly important in the case of an unsteady flow. Test conditions in short-duration wind tunnels, for instance, shock tunnels, are most similar to the model of the semi-infinite space.

The random error includes errors of measurement of flow parameters and initial temperature of the model, errors associated with insufficient knowledge of exact thermophysical characteristics of the model material, and errors of data processing algorithms.

The main sources of systematic errors include heat migration, unavailability of the recovery temperature T_e, changes in temperature of the model surface over the model length (non-isothermality), and finite thickness of the thermal indicator layer.

An analysis of accuracy of determining the heat-transfer coefficients shows that the maximum contribution to the error is made by errors of determining the parameters T_e, T_{in}, and P_0. Therefore, the total error of determining the heat-transfer coefficients is usually ~15%.

Multiple comparisons of the heat-transfer coefficients measured in our wind tunnels by thermal indicators and thermocouples are fairly satisfactory. As an example, Fig. 11 shows

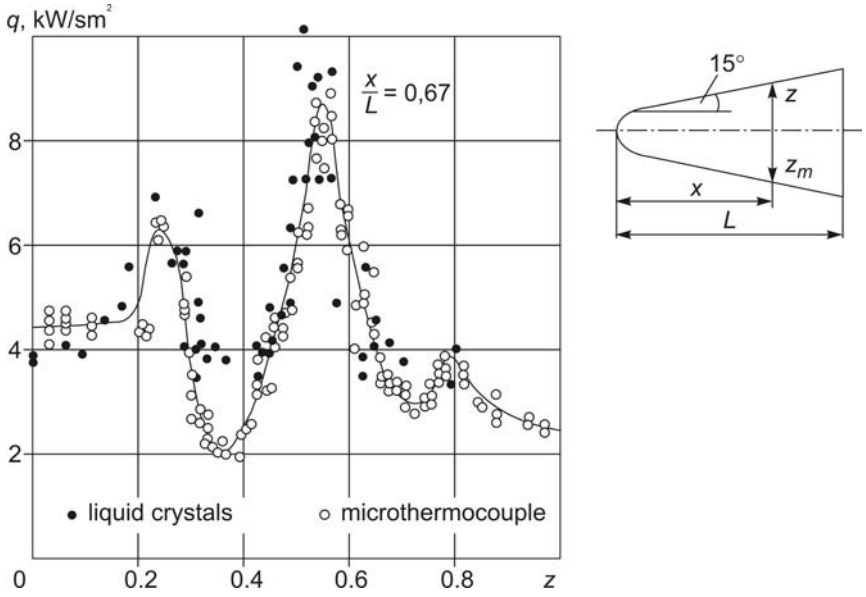

Fig. 11 Comparison of heat fluxes measured on a flat surface of a half-cone by a liquid crystal thermal indicator and by micro thermocouples ($M_\infty = 6.1$, $Re_{\infty L} = 11\times10^6$, $\alpha = 0$).

the good agreement between the heat fluxes measured by a liquid-crystal coating and micro thermocouples [23].

Method of heat-flux measurement based on infrared imaging which are widely used to visualize temperature and heat-flux fields [24, 25]. As it is known the physical essence of this method is registration of infrared radiation by a radiation detector – infrared imager. It allows scanning the image and recording the distribution of radiation intensity over the surface. Advanced infrared imagers provide a sufficiently high spatial resolution and acceptable scanning rate. The measurement accuracy is increased by calibrating the measurement system by a standard emitter, e.g., a blackbody, with subsequent correction in the course of registration and processing of information obtained. Figure 12 shows a sketch of heat-flux measurements on a flat plate. To improve the spectral properties of permeability, the glass used for windows in the test section are made of CaF_2.

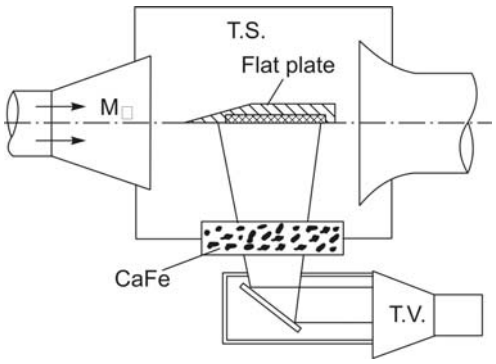

Fig. 12 Heat-flux measurements with an infrared imager

The advantages of this method are high information content, absence of thermal and gas-dynamic disturbances inherent in contact methods of measurement, and absence of problems in automation of data acquisition and processing.

The drawbacks of this method are the lower resolution, as compared with the method of thermal indicator coatings, and lower accuracy, as compared with contact temperature and heat-flux probes.

If a faster response is needed (more frequent changes of images), for instance, in experiments in short-duration facilities, the study can be confined to line-by-line (one-dimensional) scanning. In this regime, the time of scanning along one line is lower than the

time needed to scan the entire image approximately by two orders of magnitude. Consecutive registration and processing of several frames in time allows one to measure heat-flux fields.

Heat migration along the surface being neglected, the heat flux is determined by the rate of temperature variation, i.e., by the relation $q = \rho\delta C_p\, dT_w/dt$ where ρ and C_p are the density and heat capacity of the wall material, δ is the wall thickness, and T_w is the temperature of the model surface. It is better to perform heat-flux measurements on models made of heat-insulation materials.

The method of heat-flux measurements becomes more complicated if it is necessary to study heating of spatial models, because the angle of the emission direction can vary from 0 to $\pi/2$.

To make reference between the values of temperature and particular points on the surface, it is necessary to use a computer module that describes the geometry of spatial models. In this case, the slope of the emitting surface can be taken into account in processing the measured results.

If higher spatial resolution of the infrared imager is needed, especially in problems with high spatial gradients, one can use methods of image reconstruction with Fourier transforms.

The errors inherent in all heat-flux measurement methods, which are of particular importance for separated and transient flows, are the errors associated with transferring the heat-transfer coefficients obtained in wind-tunnel tests to natural conditions. These errors are related to specific features of the wind-tunnel flow, non isothermal surface of the model, and uncertainty of local temperature.

Optical method of heat-flux measurement. A new method of heat-flux measurement has been recently proposed and implemented at ITAM [26]. It is based on measuring the optical path due to change in temperature in the layer of a transparent substance, which is actually the heat-flux gauge. A scheme of this method is shown in fig. 13. A collimated beam of coherent radiation A_0 is incident onto a transparent plane-parallel plate of thickness L at an angle γ. Part of radiation is reflected from the frontal face of the plate P_2, and the other part of radiation is refracted, passes through the plate, and is reflected from the rear face P_1. Hence, reflected radiation contains two plane waves A_1 and A_2 with a phase difference $\delta\varphi$ determined by the difference in the optical path ΔS. According to optical laws, this phase difference equals $\delta\varphi = \delta\theta + 2\pi\Delta S/\lambda$, where λ is the wavelength of radiation and $\delta\theta$ is a quantity that takes into account the change in phase of the light wave due to its reflection from the interface between two media.

The temperature in the glass layer changes under the action of the heat flux Q. This leads to thermal expansion and to a change in the refractive index, thus, changing the optical path of the light wave inside the plate and, as a consequence, changing the interference pattern. This is supported by fragments of interferograms obtained during heat-flux registration (Fig. 13). The upper and lower fragments refer to times before the flow is applied and some time after the flow is applied. As was demonstrated in [26], the shift of interference fringes in two interferograms recorded after a certain time interval uniquely determines the heat flux in the corresponding region on

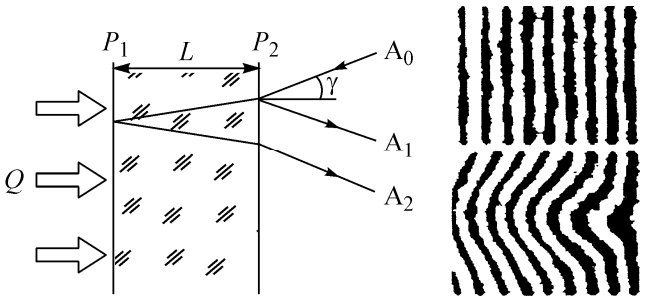

Fig. 13 Scheme of the optical method (left) and fragments of interferograms (right).

the surface as $Q(x,y) = k\dfrac{dN(x,y)}{dt}$, where $k = \lambda\rho C_p / 2(\beta + n\alpha)$ is a constant coefficient depending on the properties of the gauge material and N is the number of the interference fringe. The main sources of errors in this method are: the random error of determining ΔN; heat migration along the gauge surface; effects of elasticity and associated effects of photoelasticity and heat loss from the gauge volume.

Inaccurate determination of the shift of interference fringes is caused by noise of recorded interferograms and by insufficient spatial resolution of the cameras used. Therefore, special techniques and algorithms of Interferogram processing are needed to improve the accuracy of determining the value of ΔN.

Heat migration along the surface is inherent in all known discrete and panoramic methods of heat-flux measurement. This factor affects the error of determining local heat fluxes in regions with high temperature gradients, thus, restricting the spatial resolution of the method. To increase the accuracy, therefore, it is extremely important to define the acceptable time of registration in each case, as well as the structure and properties of the material used for the gauge.

The heat-flux gauge is usually fixed onto the model surface; hence heat migration into the model body cannot be excluded. Therefore, the measurement accuracy can be improved by increasing the gauge thickness L, which increases the spatial resolution and reduces heat loss from the gauge surface adjacent to the model. It was shown, nevertheless, in the case of a Plexiglas gauge, the depth of the heat marks does not exceed 1 mm during the time $\Delta t \approx 2$ s.

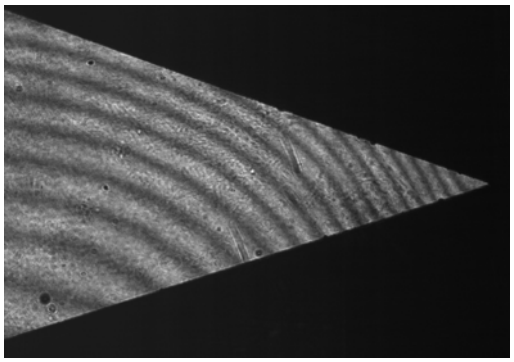

Fig. 14 Typical Interferogram obtained by measuring the heat fluxes on the windward surface of a delta wing at M∞ = 21, α = 5°

Metrological certification of the method considered was performed by estimating possible errors and by comparing the results of heat fluxes measured by calorimetric (thermocouple) and optical gauges. The difference in heat fluxes measured under identical conditions and averaged over two test series is within 5 %. Figure 14 shows a typical Interferogram obtained by measuring the heat fluxes on the windward surface of a delta wing with optical gauges.

A lot of interferograms were obtained in different tests and in different cross sections along the wing centerline and over the wing span, verifies that the error of determining heat fluxes is ±5 % if the error of measuring the shift of fringes is $\Delta N = 0.05$.

Thus, the new optical method undoubtedly expands the range of experimental methods of heat-flux measurement. The test experiments verify that the method is extremely promising.

5. Panoramic optical methods of flow visualization

Shadowgraph and schlieren visualization. It is well known that shadowgraph and schlieren methods are based on the dependence of the refractive index of gases on density $n = 1 + \xi\rho$, where n is the refractive index, ξ is the Gladstone-Dale constant, and ρ is the gas density. These methods are widely used in all aerodynamic laboratories, based on standard shadowgraphs. These devices are highly sensitive, which is extremely important in studying

hypersonic flows with low densities of the gas flow in the test section. Shadowgraph, where the displacement of a light beam that passed through an inhomogeneity is registered, are mainly used to visualize the flow structure, whereas schlieren methods (developed by August Toepler), which make it possible to register density gradients, are also widely used for obtaining quantitative information on density fields. These methods have been known for a long time and are described in numerous publications.

In schlieren devices, a quasi-parallel light beam that passed through an inhomogeneity is focused by a lens in the plane of the Foucault knife where the slot image is formed. The so-called Toepler devices based on this principle are the most widely used optical instruments for aerodynamic experiments. In studying flows with small density gradients, however, there are substantial constraints. In particular, the use of devices with the Foucault knife is ineffective in hypersonic flows, which are characterized by extremely small variations of density (less than 10^{-3} of the atmospheric density). The same problem arises in measurements in near-wall flows with characteristic velocities of ≤ 10 m/s, where the change in density is $\frac{\Delta\rho}{\rho_0} \approx 10^{-5}$. To solve this problem, A.A. Pavlov at ITAM proposed to use an adaptive visualization transparent (AVT) instead of the Foucault knife [26, 27]. In this case, the transparent is made of a phototropic material (e.g., silica glass with silver halide microcrystal), which is darkened to an extent depending on intensity of focused radiation. A typical feature of such materials is an extremely high spatial resolution. Probing radiation experiencing small angular deviations on weak inhomogeneities passes through the non-darkened part of the AVT and can be seen on the schlieren picture as a brighter area. Flow visualization is performed with the conventional optical scheme of the schlieren device shown in Fig. 15. In this scheme, radiation from the laser 1 is formed into a plane-parallel beam with the help of the lenses 2 and 3. This beam passes through the inhomogeneity 4 and then is focused by the lens 5 in the focal plane 6, where a thin plate 9 made of phototropic glass (AVT) is located. After that, the inhomogeneity image is focused by the lens 7 in the plane of the photodetector 8. In this case the AVT area in the focusing region is darkened, and the main part of radiation is absorbed. For this reason the overall background of the image becomes dark. Radiation that was deflected on the inhomogeneity passes through the non-darkened area of the AVT and is seen in the image as a lighter area. Coincidence of the darkened area and light source image sizes is ensured automatically, and a high resolution of the AVT ensures the minimum possible size of the visualization spot.

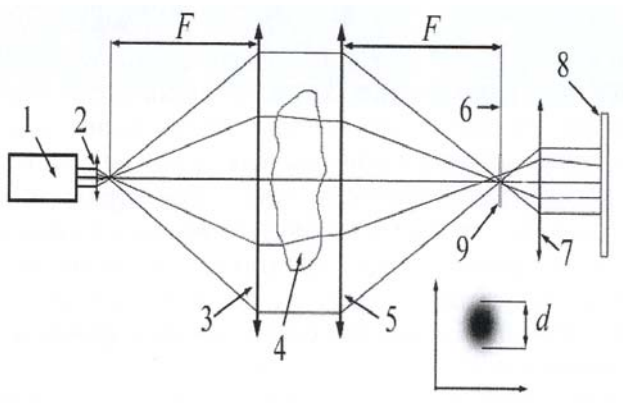

Fig. 15 Schlieren device with an adaptive visualization transparent.

Thus AVT method allows to getting qualitatively different results at supersonic flows since permit visualizes weak inhomogeneity on the background of the strong density gradients which is difficult for usually used Schlieren devices.

An example of using this method show that the visualization spot approximately 10 μm in size allows registration of deflection angles $\Delta\alpha_{\min} \approx 5 \cdot 10^{-8}$. The sensitivity of this method is higher approximately by two orders of magnitude than that of the standard schlieren technique. Therefore,

this method is widely used to visualize weak inhomogeneity of various flow regimes. Figure 16 shows the comparison of visualization a streamwise flow with the bow shock wave generated by a downstream located end face of a cylinder by using AVT and usual Foucault knife methods. The images obtained by two different methods are obviously different. Therefore, the use of the AVT sometimes allows qualitatively different information to be obtained. An undoubted advantage of this method is the AVT adaptation (automatic tuning of transmission), which simplifies arrangement of experiments.

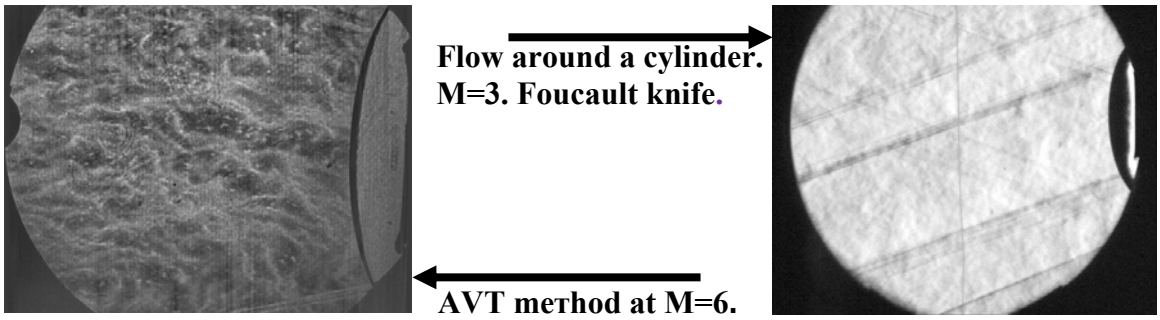

Fig.16 Using the adaptive visualization transparent (AVT) at supersonic flows

Laser-sheet method is one of the widespread methods of visualization of the flow structure, vortices, and shock-wave interactions in a chosen section, which is based on the vapor screen [29]. The operation principle of this method is based on scattering of laser radiation on particles contained in the flow. The intensity of this radiation is proportional to the concentration of in the examined section. But the majority wind tunnels operate on pure dried air without any particles, which incurs problems that were successfully solved in [30]. One possible optical scheme is shown in Fig. 17, where the probing light beam *2* from the laser *1* is expanded by the negative lens *3*, is reflected from the mirror *4*, is expanded along the coordinate by the cylindrical lens 5, and is inserted into the collimator part of the standard schlieren instrument. At the output, this device forms a "laser-sheet" light beam less than 1mm thick. After that, passing through the positive spherical lens, the light beam forms a focal plane that crosses the examined region, thus, providing the minimum thickness of the laser sheet. The flow formed in this section is registered by the photo or video camera *9*.

The laser-sheet method is intensely used in our wind tunnels. As an example, Fig. 18 shows a typical image of the flow around a delta wing with clear expose all peculiarities: location of the bow shock *2*; the vortex sheet *3* which coils into the primary vortex *4*; the

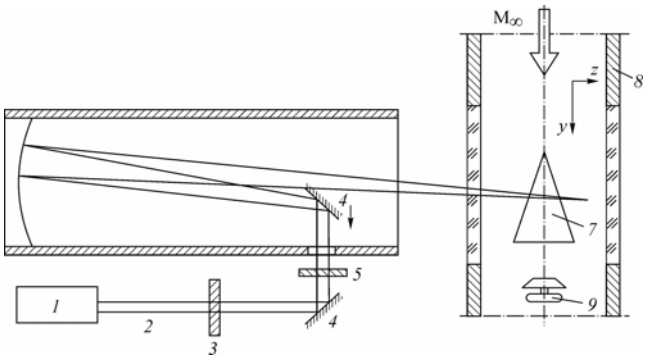

Fig. 17 Sketch of laser-sheet

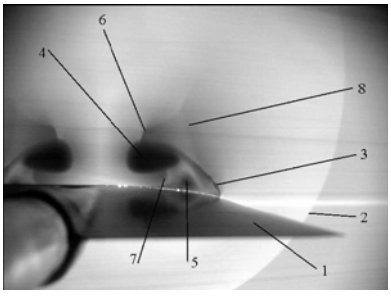

Fig. 18 An image of the flow around a dta wing

formation of a secondary vortex *5*; hanging shocks *6* and *7*; as well as the λ – shock *8* formed above the vortex sheet and the primary vortex.

There are all grounds to believe that further development of the laser-sheet method will ensure successful visualization of the flow in impulse tunnels.

Interferometry with formation of a reference beam from an individual light source.

It is commonly known that interferometry offers the most effective optical methods for studying gas flows, because they allow quantification of density distributions in some classes of flows. Various types of these methods are used in aerodynamic laboratories. It is known, however, that the basic feature of two-beam interferometers is the use of one light source for forming both the object and reference waves [31–33]. Therefore, the use of interferometers with amplitude splitting of the beams usually involves significant technical difficulties, which restrict wide application of optical interferometry despite its effectiveness.

To solve this problem, Pavlov A.A proposed a method of registration interferograms of phase objects with the reference wave being formed from another light source, which allows substantial extension of the possibilities of using interferometry.

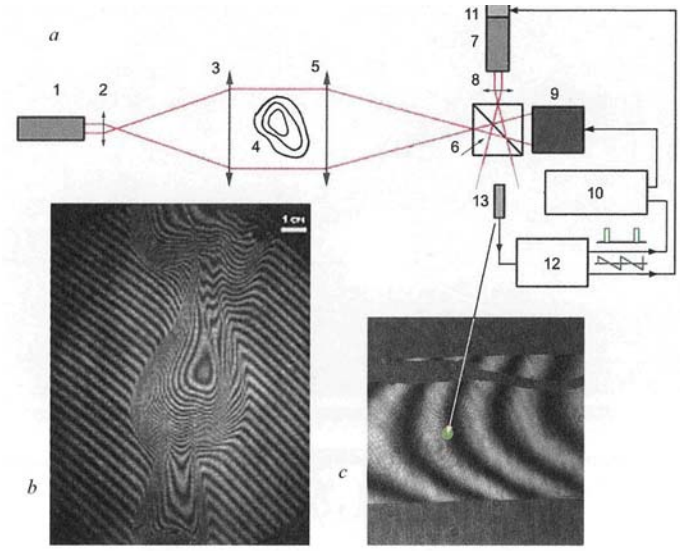

Fig. 19

Figure 19 shows the principal diagram of the optical system for obtaining interferograms from two independent light sources. The probing radiation from the He–Ne laser 1 by the lens *2* and the collimating lens *3* is formed into a plane-parallel beam, which is the object wave. After passing through a phase inhomogeneity and the collecting lens *5*, this radiation goes to Fig. 19 the registration device consisting of a LED cube (light splitter) *6*, a laser source of light *7* with a lens *8*, and a TV camera. To obtain high-quality interferograms, one of the mirrors of the laser *7* is mounted on a piezoceramic bushing *11* to which a saw-tooth voltage with an amplitude of 12 V is supplied from a digital oscillograph/generator *12*. Whis using computer *10* and a photosensor *13* it is possible to change the voltage on the piezoceramic bushing which leads to a change in the laser radiation frequency.

The signal from the sensor is used for synchronization of TV camera actuation. The lasers and the TV camera are adjusted so that the frequency of one of the lasers could be

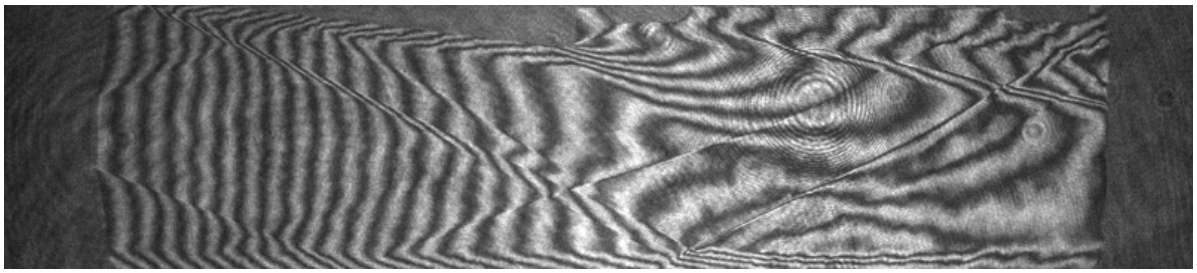

Fig. 20 Flow around a wedge at M∞ = 3.

shifted by changing the cavity temperature; as a result, 1–3 interference patterns can be registered. A typical ineterferogram of the alcohol burner flame obtained by this method is shown in Fig. 19*b*. Another example of registration of interferograms of the flow around a wedge at $M_\infty = 3$, used further to calculate the density, is shown in Fig. 20.

This method can be used almost in all facilities equipped with the schlieren instrument.

References

1. Pope A. and Goin K., High-Speed Wind Tunnel Testing, Krieger Publishing Company, 1965.
2. Petunin A.N. Methods and Techniques of Measuring Gas-Flow Parameters [in Russian], Mashinostroenie, Moscow, 1996.
3. Kharitonov A.M. Techniques and methods of Aerophysical experiments Part 2 Methods and facilities of Aerophysical measurements [in Russian], NSTU, Novosibirsk, 2007.
4. Latypov A.F. Method of determination the force and heat-flaxes characteristics of the models by testing in the impulse facilities J. of Appl. Mech. and Tech. Phys., Vol. 47, No. 5, 2006, pp.47-55.
5. Gounko Yu.P., Kharitonov A.M., Latypov A.F., Mazhul I.I., Yaroslavtsev M.I. Technique for determination of heat fluxes and force characteristics of ramjet/scramjet models in a hot-shot wind tunnel, Proc. of Int. Conf. on the Methods of Aerophysical Research, Part 3, Novosibirsk, 2000, pp. 51–56.
6. Prandtl L., Hydro aeromechanics [Russian translation], Research Center "Regular and Random Dynamics," Moscow, 2000.
7. Zheltovodov A.A., Kornilov V.I., Kharitonov A.M. in: Kharitonov A.M. (ed.), Methods and Techniques of Aerophysical Research, Collected papers of ITAM, Novosibirsk, 1978, pp. 26–43.
8. Brodetsky M.D., Kharitonov A.M., Shevchenko A.M., et al., On the method of measuring the direction and Mach number of a three-dimensional supersonic flow, Uch. Zap. TsAGI, Vol. XV, No. 3, 1984.
9. Tavoularis S. Measurement in Fluid Mechanics, Cambridge University Press, 2005.
10. Nesterikhin Yu.E., Soloukhin R.I., Methods of Velocity Measurements in Gas Dynamics and Plasma Physics [in Russian], Izd. Novosib. Gos. Univ., Novosibirsk, 1965.
11. Alievskaya A.N., Mironov Yu.V., Slezinger I.I., Shiryaev V.A., Automated measurement and computational unit for pressure measurements in a supersonic wind tunnel, Trudy CIAM, No. 972, 1982, pp. 170–195.
12. Ardasheva M.M., Nevsky L.B., Pervushin G.E., Method of pressure distribution visualization with the organic luminophores, Proc. III USSR School on the Methods of Aerophisical Investigations, Novosibirsk, 1982, pp. 103–107.
13. Ardasheva M.M., Nevsky L.B., Pervushin G.E., Method of pressure distribution measurement with the indicating, J. of Appl. Mech. Tech. Phys., No. 4, 1985.
14. Zharkova G.M., Maksimov A.I., Pavlov A.A., Khachaturyan V.M., Pressure visualization on aerodynamic surface by the method of luminescent coating, Proc. 6th Intern. Symposium "Flow Visualization", Yokohama, Japan, 1992, pp. 613–622.
15. Boshnyak L.L. Measurement in Heat Engineering Research [in Russian], Mashinostroenie, Leningrad, 1974.
16. Zharkova G.M., Sonin A.S., Liquid Crystal Composites [in Russian], Nauka, Novosibirsk, 1994.

17. Zharkova G.M., Optical phenomena in liquid crystals and their application in aerophysical studies, Optical & Laser Technology, 2000, 32, pp. 611-619.
18. Zharkova G.M., Kovrizhina V.N., Kornilov V.I., Pavlov A.A., Method of registration of temperature fields with the use of liquid crystal coatings, Thermophys. and Aeromech., 1996. Vol. 3, No. 4.
19. Kuznetsov Yu.E., Gudilin I.V., Errors of measuring the convective heat flux by small-size probes, Tr. TsAGI, No. 2388, 1988.
20. Sapozhnikov S.Z., Mityakov V.Yu., Mityakov A.V., Gradient-Type Heat-Flux Probes, Izd. SPbGPU, St. Petersburg, 2003.
21. Knauss H., Gaisbauer U., Wagner S., Buntin D., Maslov A., Smorodsky D., Betz J., Calibration experiments of a new active fast response heat flux sensor to measure total temperature fluctuation, Proc. Intern. Conf. on the Methods of Aerophys. Research, Pt. III, Novosibirsk, 2002, pp.86–113.
22. Brazhko V.N., Kovaleva N.A., Maikapar G.I., On the method of heat-flux measurement with the use of thermal indicator coatings, Uch. Zap. TsAGI, Vol. XX, No. 1, 1989.
23. Borovoi V.Ya., Gas Flow and Heat Transfer in Zones of Shock Wave-Boundary Layer Interaction [in Russian], Mashinostroenie, Moscow, 1983.
24. Bashurov V.V., Boichuk L.N., Vorontsov S.S., Vyshenkov Yu.I., Modular infrared imager TV-M, in: Infrared Imaging (collected papers) [in Russian], MIREA, Moscow, No. 6, 1986.
25. Carlomagno G.M., de Luca L., Infrared thermography application in convective heat transfer, Multiphase Flow visualization 5, Hemisphere, 1990, pp. 843–848.
26. Golubev M.P., Pavlov A.A., Pavlov Al.A., Shiplyuk A.N., Optical method of heat-flux registration, J. Appl. Mech. Tech. Phys., Vol. 44, No. 4, 2003.
27. Pavlov A.A., Pavlov Al.A., Golubev M .P. and others, Schlieren device with an adaptive visualization transparent AVT for investigation of flow disturbances creation by optical pulse discharge in gases // Proc. IX Int. Conf. OMIP-2007, M., MEI, pp.174-177.
28. Pavlov A.A., Pavlov Al.A., Golubev M .P., Schlieren device with an adaptive visualization transparent. // Proc. IX Int. Conf. OMIP-2007, M., MEI, pp.170-173.
29. Gregor Mc., The Vapour- Screen Method of Visualization // J. Fl. Mech. Vol.11, No. 4, 1961, pp.481-511.
30. Maksimov A.I., Pavlov A.A., Development of Laser-sheet method for flow visualization in supersonic wind tunnels // Uch. Zap. TsAGI, Vol. XX, No. 1, 1986.
31. Pavlov A.A., Pavlov Al.A., Golubev M.P., Method of phase Heterogeneity Interferogram Registration with a Reference Beam Forming from a separate Light Source // Proc. XII Int. Conf. on the Methods of Aerophysical Research., Vol. 2, Novosibirsk, 2004, pp. 157-161.
32. Pavlov A.A., Pavlov Al.A., Golubev M .P., Interferogram Registration with a Reference Beam Forming from a separate Light Source // 12th Int. Symp. on Flow Visualization (ISFV-12). Goettingen, Germany, Art. №154, 2006
33. Pavlov A.A., Pavlov Al.A., Golubev M.P., Automation of Interferogram Registration with a Reference Beam Forming from a separate Light Source // Proc. XIII Int. Conf. on the Methods of Aerophysical Research., Novosibirsk, 2007, Vol. 4, pp. 137-142.